Advances in Science and Technology Research Journal

Advances in Science and Technology Research Journal, 2025, 19(9), 393–409
https://doi.org/10.12913/22998624/207598
ISSN 2299-8624, License CC-BY 4.0

Received: 2025.05.25
Accepted: 2025.07.15
Published: 2025.08.01

Experimental and numerical verification of the influence of the covering height on the shape of equilibrium paths

Paweł Zabojszcza[1*], Urszula Radoń[1]

[1] Faculty of Civil Engineering and Architecture, Kielce University of Technology, Al. Tysiąclecia Państwa Polskiego 7, 25-314 Kielce, Poland
* Corresponding author: pawelzab@tu.kielce.pl

ABSTRACT

The proper definition of the numerical model of the analysed structure is one of the key task of structural design. It is essential that the description of numerical models differs as little as possible from the actual behaviour of the structure. For this reason, it is extremely important to be able to verify and calibrate numerical models using experimental studies. This article includes a series of experimental tests and numerical analyses for two types of steel bar domes. The structures differ in height. The aim of this study was to calibrate a numerical model of a dome structure by incorporating relevant geometric nonlinearities and fabrication imperfections, in order to match experimental results. The numerical simulations were conducted in Abaqus using geometrically nonlinear analysis with the Riks method, which enables tracking the full equilibrium path, including buckling and snap-through phenomena. Initial simulation results deviated significantly from experimental observations, particularly in terms of the keystone node displacement and the load-displacement relationship. To determine the source of discrepancies, a detailed investigation was carried out, focusing on boundary conditions, fabrication quality, and support compliance. Slight settlement was observed at the supports, which indicated the need to introduce elastic supports into the numerical model. Additionally, geometric imperfections were implemented in the form of the first buckling mode with a realistic amplitude, in accordance with design standards. The incorporation of both elastic support conditions and geometric imperfections led to a substantial improvement in the correlation between numerical and experimental results. The study demonstrates that even small-scale local effects, such as settlement or member imperfections, can significantly influence the global structural response. The obtained static equilibrium paths for the high-rise and low-rise coverings differ significantly. The linear analysis with linear buckling analysis work well for the high-rise dome. For the low-rise dome, a nonlinear analysis was necessary. These structures are subjected to large displacement gradients, and the analysis of the equilibrium path in the range of geometric nonlinearity is essential.

Keywords: steel covering, finite element method, stability loss, equilibrium path, support flexibility, geometrical imperfections.

INTRODUCTION

Steel bar covers are spatial structures consisting of a system of interconnected steel bars, creating a rigid and durable geometric grid. Single-layer steel bar covers are widely used in industrial halls, warehouses or sports facilities [1-3]. In the design of bar coverings, an important parameter is their height, often defined as the ratio of height to span. The value of this parameter affects the distribution of internal forces generated in the structure. The article [4] emphasized that spatial bar structural coverings is a popular method of roofing large areas, enabling the use of a small number of intermediate supports, and their height affects the efficiency of the structure. The article [5] indicates that in the case of multi-layer structural roofs, the ratio of the structure's height to its span is usually in the range of 1/60–1/100, and in the case of shell structures this ratio can be much smaller. Moreover, the article [6] discusses various types of coverings, such as mesh domes and grates, which differ in their prominence and shape, which affects their structural properties. Single-layer bar coverings exhibit

complex responses to loads, which are reflected in the equilibrium paths. Analysis of static equilibrium paths allows determining the behaviour of these structures under various loading conditions. Nowadays, modern, numerical techniques provide a computational tools to study the behaviour of engineering structures. In the paper [7] Authors show an experimental path-following method that uses Newton's method, stiffness and residual forces to continue along unstable and stable equilibrium paths. The paper [8] describes experimental and numerical analysis of the post-buckling behaviour of geodesic lattice domes. The paper [9] describes a numerical methodology for the geometrically nonlinear analysis of structures under unilateral contact constraints. The nonlinear problem contains two distinct types of variables: the length, position of the contact regions and the displacement field. To solve the system of nonlinear algebraic equations with contact constraints and determine the structural equilibrium configuration, the authors propose a two-level iterative solution strategy for each load increment. In the first stage, the contact problem is addressed as a linear complementarity problem using Lemke's algorithm, followed by updating the displacement field in the second stage. In paper [10], four reticulated shell models incorporating roofing systems are experimentally analysed to assess the influence of the roofing system. Finite element method (FEM) simulations were developed based on these experimental models to validate the numerical findings. The paper [11] examines how the buckling load of a single-layer covering stiffened with cables will change compared to a covering without cables. The following parameters were taken into account in the analysis: cable routing methods, types of connections, prestress in cables, and cable cross-sections. The results indicate that the buckling load of single-layer gratings has been significantly improved by introducing cables. In the paper [12] nonlinear and linear seismic responses of single-layer Kiewitt dome are estimated. Computations of the structural analysis are implemented in ANSYS. The authors demonstrate that relying on only seven ground motion record components in seismic design can result in either overestimation or underestimation of structural performance. They recommend using a greater number of ground motion records to reduce the relative differences observed in failure probabilities and improve the reliability of seismic design. In [13], both numerical and experimental studies are conducted on gear-bolt joints used in grid spatial structures. A series of monotonic loading tests are performed on the gear joints to evaluate their performance. The experimental setup allows for direct assessment of the impact of several critical parameters, including ball thickness, gear bolt diameter, the ratio of tooth depth to bolt diameter, and the number of teeth. FEM model of the gear joints is verified by the experimental results. In the paper [14] is proposed a new parameter to assess global stability analysis of structures. This parameter is mathematically derived from the incremental equilibrium equation of the nonlinear stability analysis. Equilibrium paths with detailed geometrically and materially nonlinear analysis for single-layer reticulated domes are described. Interesting study on progressive collapse of single-layer latticed domes is described in [15]. Numerical simulations and experimental tests are carried out to understand the way of internal force redistribution during the collapse of the Lamella and geodesic domes. Three effective methods to evaluate collapse resistance are described. Ensuring the overall stability of the structure is extremely important from the point of view of safety and reliability. Problems of stability loss are a common topic of research by scientists, including Silva and Ribeiro [16]. In the works [17, 18] the authors present numerical simulations along with detailed experimental studies of the collapse resistance of single-layer lattice domes. The simulations of equilibrium paths taking into account the nonlinear finite element model were presented in [19]. The issues related to the response to dynamic actions of most designed structures are as important to consider during design as the stability analysis. In the works [20–22] the authors tried to present various aspects of the influence of dynamic analysis on the structure.

In the evaluation of the performance of steel bar coverings, an extremely important issue is the correct determination of the numerical model of the analysed structure. The accuracy of these models may differ from the actual behaviour of the structure. For this reason, it is necessary to verify and calibrate them using experimental tests. Experimental analysis involves physical testing of a structure to investigate its actual behaviour under load. To achieve this goal, we use static and dynamic tests, which are performed in laboratories or in the field. These tests involve applying loads and monitoring their effect on the structure. The advantage of experimental analysis is the direct consideration of the actual operating conditions of the structure, such as material imperfections or

manufacturing errors. Experimental results can reveal unexpected behaviours of the structure that were not included in the numerical models (e.g. the effect of material variability or manufacturing errors). Results obtained by the experimental method increase confidence in the results obtained using numerical simulations.

Numerical analysis, most often using the FEM, allows for modelling complex steel structures. This method allows for simulation of the behaviour of the structure in various conditions, taking into account the description of the complex geometry of the structure, nonlinear material properties, boundary conditions and load. Numerical analysis allows for quick changes in the structure model, e.g. modification of geometry or material, which in the case of experimental studies requires a lot of time and money. A major advantage of this method is the ability to perform simulations in many load variants and boundary conditions without the need to build physical models. At the stage of numerical simulations, it is also possible to optimize the structure. Conducting an analysis for different variants of the geometry and load of the structure allows for optimizing the design in terms of strength, mass and costs. However, this method is not free from drawbacks. Errors in the numerical model can lead to incorrect interpretation of the behaviour of the structure in real conditions.

This article includes a series of experimental tests and numerical analyses for two types of steel bar domes. The structures differ in height. The aim of this study was to calibrate a numerical model of a dome structure by incorporating relevant geometric nonlinearities and fabrication imperfections, in order to match experimental results. In the numerical model of the dome structure, spatial frame elements were used. The numerical calculations were performed in the Abaqus environment using a geometrically nonlinear analysis with the Riks method, which enables capturing buckling and snap-through phenomena as well as obtaining the full equilibrium path within the instability region.

At the initial stage of the study, the numerical results differed significantly from the experimental data. The discrepancies concerned both the displacement values of the keystone node and the shape of the load-displacement curve. To identify the sources of these differences, a detailed inspection of the test setup was carried out, focusing on:

- the method of fixing the structure in the test stand,
- possible deformations or manufacturing deviations of the structural elements,
- the actual stiffness of the supports.

During testing, slight settlement was observed at the support location, likely resulting from material deformation or deformation of the connection to the base. This indicated that the initially assumed perfectly rigid supports did not reflect the real behavior of the structure. Consequently, modifications were introduced to the numerical model by implementing elastic supports, defined by an appropriate translational stiffness. This allowed the model to reflect the compliance of the support node to vertical displacements, bringing the numerical results closer to the experimental measurements.

Another significant step involved the inclusion of geometric imperfections. A characteristic imperfection shape in the form of the first buckling mode was adopted, with a realistic amplitude consistent with design standards. The inclusion of these imperfections had a considerable effect on the structural response, particularly in terms of initial stiffness and the onset of geometric instability. Only after accounting for both factors – elastic supports and real geometry with imperfections was satisfactory agreement between the experiment and the numerical simulation achieved. This applied to both the keystone node displacement values at various load levels and the overall shape of the load-displacement path.

The structure of the paper is as follows. After a short introduction, the concept of equilibrium path is defined. Then, the tools necessary to perform numerical simulations are described. The next chapter concerns the detailed description of the measuring stand. Then, the results of experimental and numerical studies are presented. The paper ends with a discussion of the obtained results and conclusions.

THE EQUILIBRIUM PATH

One of the important tasks in analysis of structure is the determination of the equilibrium path. An equilibrium path is a curve in the space of the generalized displacements and the load factor. Stability analysis of the equilibrium state can be described based on the stability condition at the stationary point of the total potential energy.

In this section we define nonlinear equilibrium equations using the potential energy of the structure $V=V(q,Q)$ as a function of a load vector Q and a displacement vector q. We assume that vector Q is a proportional, one-parameter load:

$$Q = \mu \cdot P \tag{1}$$

where: μ – load multiplier, P – comparative load vector.

Change of parameter μ leads to changes of the displacement vector q. The next solutions generate in an (N+1) dimensional space $(q_1,q_2,\ldots,q_N, \mu)$ a curve called an equilibrium path. We choose a point $A(\tilde{q},\tilde{\mu})$ on the equilibrium path. The point $A(\tilde{q},\tilde{\mu})$ is not a singular point nor to its vicinity. We will describe the change of the system state by the change of μ parameter. We will describe a new point $B(\tilde{q}+\Delta q,\tilde{\mu}+\Delta\tilde{\mu})$ on the equilibrium path.The potential energy at B point close to A point we can write:

$$\begin{gathered} V_B = V(\tilde{q}+\Delta q,\tilde{\mu}+\Delta\tilde{\mu}) = V(\tilde{q},\tilde{\mu}) + \\ + \frac{\partial V(\tilde{q},\tilde{\mu})}{\partial q}\Delta q + \frac{\partial V(\tilde{q},\tilde{\mu})}{\partial \mu}\Delta\mu + \\ \frac{1}{2!}\left[\begin{array}{c}\frac{\partial^2 V(\tilde{q},\tilde{\mu})}{\partial q^2}(\Delta q)^2 + 2\frac{\partial^2 V(\tilde{q},\tilde{\mu})}{\partial q\partial\mu}\Delta q\Delta\mu + \\ + \frac{\partial^2 V(\tilde{q},\tilde{\mu})}{\partial \mu^2}(\Delta\mu)^2\end{array}\right] + \cdots + \\ + \frac{1}{n!}\left[\sum\binom{n}{k}\frac{\partial^n V(\tilde{q},\tilde{\mu})}{\partial q^{n-k}\partial\mu^k}(\Delta q)^{n-k}(\Delta\mu^k)\right] \end{gathered} \tag{2}$$

The first derivative of potential energy V in the vicinity of A point takes the form:

$$\begin{gathered} \frac{\partial V_B}{\partial q} = \frac{\partial V(\tilde{q}+\Delta q,\tilde{\mu}+\Delta\tilde{\mu})}{\partial q} = \\ = \left[\frac{\partial^2 V(\tilde{q},\tilde{\mu})}{\partial q^2}\Delta q + \frac{\partial^2 V(\tilde{q},\tilde{\mu})}{\partial q\partial\mu}\Delta\mu\right] = \\ + \frac{1}{2!}\left[\begin{array}{c}\frac{\partial^3 V(\tilde{q},\tilde{\mu})}{\partial q\partial\mu^2}(\Delta\mu)^2 + 2\frac{\partial^3 V(\tilde{q},\tilde{\mu})}{\partial q^2\partial\mu}\Delta q\Delta\mu + \\ + \frac{\partial^3 V(\tilde{q},\tilde{\mu})}{\partial q^2}(\Delta q)^2\end{array}\right] + \cdots \end{gathered} \tag{3}$$

Assuming the configuration $(\tilde{q}+\Delta q)$ i $(\tilde{\mu}+\Delta\mu)$ to be also an equilibrium state and neglecting the nonlinear term of the increments Δq and $\Delta\mu$ the linearized incremental equations set takes the form:

$$\frac{\partial^2 V(\tilde{q},\tilde{\mu})}{\partial q^2}\Delta q + \frac{\partial^2 V(\tilde{q},\tilde{\mu})}{\partial q\partial\mu}\Delta\mu = 0 \tag{4}$$

According to Castigliano's theorem, if an external load Q is conservative, we can write:

$$-P = \frac{\partial^2 V(\tilde{q},\tilde{\mu})}{\partial q\partial\mu} \tag{5}$$

The set of nonlinear equations (4) in the matrix version takes the form:

$$K_T(q,\mu)\cdot\Delta q - \Delta\mu P = 0 \tag{6}$$

where: $\frac{\partial^2 V(\tilde{q},\tilde{\mu})}{\partial q^2} = K_T$ – tangent stiffness matrix of the structure.

The set of nonlinear algebraic equations, we can compute using incremental-iterative Newton-Raphson methods. During iteration, at each incremental step, we can write:

$$K_T(q)\cdot\Delta q = \Delta\mu \cdot P + R \tag{7}$$

where: $K_T(q)$ – tangent stiffness matrix of the structure, $R=P-F$ – vector of residual forces, F – vector of internal forces.

In the equilibrium state $R = 0$, while in the iterative process the R standard defines the distance from the equilibrium state. The iterative process converges if $R > 0$.

The matrix K_T of the structure is created as a result of aggregation stiffness matrix of the elements K_T^e:

$$K_T = \sum_{i=1}^{e} K_T^e = \sum_{i=1}^{e} (K_L^e + K_G^e + K_{u1}^e + K_{u2}^e) \tag{8}$$

where: K_L^e is the tangent stiffness matrix of the element composed of linear stiffness matrix K_L^e, geometric stiffness matrix K_G^e and nonlinear stiffness matrices: K_{u1}^e and K_{u2}^e.

DESCRIPTION OF THE NUMERICAL TOOLS

The Equations 7 define a curve, called the equilibrium path, in N+1 dimensional space {q, μ}. The determination of the load-displacement relationship is closely related to the singularities along this curve. The singular points are defined as critical points, including the limit point (L), bifurcation point (B), turning point (R) (Figure 1).

In the case of a low-rise covering, the equilibrium path often has a limit point. Unfortunately, the load multiplier μ is not a correct parameter for the curve with limit points. At the limit points this parameter attains the local extremum. In order to surmount effectively around the critical points, special computing techniques should be used. The most popular in practical applications is arc length method. The arc length method has been proposed by Riks [23, 24] and Wempner [25], who suggest, that arc length s can be a right choice:

$$q = q(s)\ \mu = \mu(s) \tag{9}$$

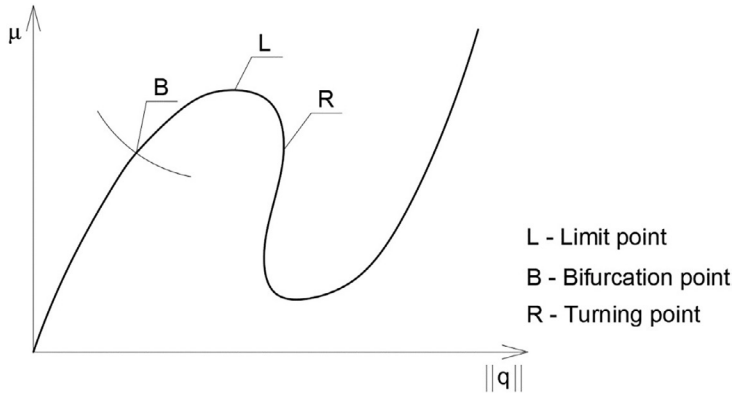

Figure 1. The equilibrium path diagram

This parameter is used as a control parameter in the incremental-iterative process. In the arc length method an additional equation (10) is added to the basic set of Equations 7.

$$\Delta s = g(\Delta q, \Delta \mu) \tag{10}$$

Equation 10 defines the arc length increase. Different approximations can be used. For constant Δs Equation 10 determines some hypersurface that intersects the equilibrium path at the next point. The difference between the standard incremental-iterative process and the constant arc-length method is illustrated in the Figure 2.

An initial point on the equilibrium path, we can find solving set of equations:

$$\begin{aligned} K_T \Delta q^{(1)} - \Delta \mu^{(1)} P &= 0 \\ \frac{\partial g}{\partial q} \Delta \mathrm{q}^{(1)} - \frac{\partial g}{\partial \mu} \Delta \mu^{(1)} &= \Delta s \end{aligned} \tag{11}$$

The next points are computed using the following iteration scheme (for Δs = const):

$$\begin{cases} K_T^{(i-1)} \delta q^{(i)} - P \delta \mu^{(i)} = \mu^{(i-1)} P - R^{(i-1)}, \\ \frac{\partial g}{\partial q} \delta \mathrm{q}^{(i)} - \frac{\partial g}{\partial \mu} \delta \mu^{(i)} = 0 \\ for\ i > 1 \end{cases} \tag{12}$$

The quantities q, μ, Δq, $\Delta \mu$ are updated in each iteration:

$$\begin{aligned} q^{(i)} &= q^{(i-1)} + \delta \mathrm{q}^{(\mathrm{i})} \\ \mu^{(i)} &= \mu^{(i-1)} + \delta \mu^{(\mathrm{i})} \\ \Delta q^{(i)} &= \Delta q^{(i-1)} + \delta \mathrm{q}^{(\mathrm{i})} \\ \Delta \mu^{(i)} &= \Delta \mu^{(i-1)} + \delta \mu^{(\mathrm{i})} \end{aligned} \tag{13}$$

The arc length method was followed by many modifications. Batoz and Dhatt [26] developed a technique of solution of the extended system of equations, preserving the symmetry of the stiffness matrix. This technique was used by Crisfield [27–29] in his spherical arc length method. Many of the later paper [30–33] concern the modifications of the control equation and an automatic governing of the incremental process. A modified Riks method by Crisfield, Ramm and Powell and Simons has been implemented in Abaqus software. This software is used in our paper.

The paper takes into account the influence of imperfections on the equilibrium path of the structure, which requires several stages in the Abaqus environment. In the first stage, the Buckle analysis was run, which results in buckling modes of the structure and the value of the critical force

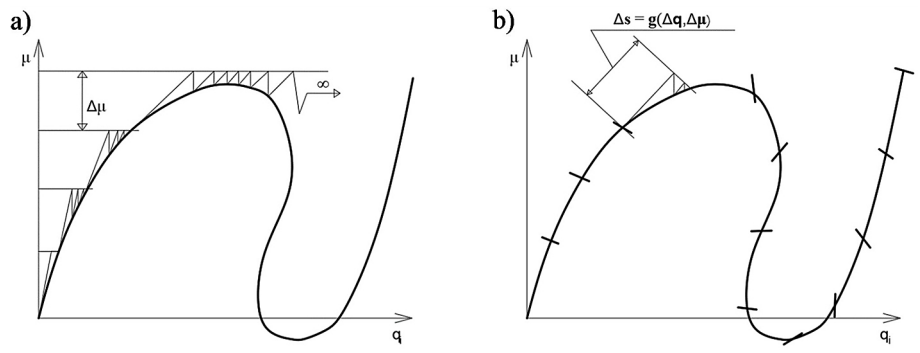

Figure 2. The incremental-iterative process: (a) standard, (b) constant arc-length method

corresponding to each of them. In the next step, the ideal geometry of the members was disturbed by the displacements of the nodes calculated in the Buckle step using the *IMPERFECTION* command and *STATIC RIKS* calculations were performed. Several different combinations of taking into account the eigenvector value of the first buckling mode were performed, for which the most optimal version was presented. The nature of the obtained equilibrium path clearly indicates an improvement in the convergence of the results [34–35]. The problems of determining the equilibrium path in deterministic and probabilistic description were also discussed in the articles [36].

Abaqus software also allows to include in the numerical model the flexibility of supports, using the *SPRING* option. The type of connection (e.g. as an elastic attachment to the substrate) is considered in the model, taking into account the spring coefficient. Spring elements are used to model real physical springs, as well as idealizations of axial or torsional elements. They can also model constraints preventing the movement of a rigid body. They are also used to represent structural dampers by specifying structural damping coefficients to create the imaginary part of the spring stiffness.

DESCRIPTION OF THE EXPERIMENTAL RESEARCH STATION

Nowadays, nonlinear structural analysis seems to be essential for most structural engineering applications. Many engineers have started to lean towards more detailed structural analysis. However, creating numerical models that better describe the actual behavior of structures requires their validation through experimental studies. In this paper, we verify their numerical models by experimentally determining the equilibrium paths of two bar covers. In this section, we describe the experimental research station.

The test stand was constructed to test the displacement of the nodes of a steel rod-shaped roof structure (bar dome). Figure 3 shows the appearance of experimental models test stand (Figure 3a) and scheme (Figure 3b), respectively. It consists of two main parts: a stable base with a load module made of steel profiles (the structure consists of C-beams and I-beams) and a solid ring made of square tubes on which the tested structure is placed. Both parts are connected with clamps during the test. The load was applied to the keystone using a hydraulic actuator. The plate was attached to a hook scale using a steel sling. The hook scale, which is mounted in the key, enables precise reading of the load that is currently applied using a ratchet hook. The displacements were read from electronic sensors (ES1). Laser levels were used to control the setting of the hydraulic actuator in two directions, which allow for precise determination of the position of the actuator during the test. Each of the models was attached to a steel ring using bolts, simulating articulated supports.

Thanks to this method, the load control and its distribution on the tested structure is precise, which allows for precise verification of the structure's response to the introduced load. PO10 and PO12 steel rods were used to make the tested structure (Figure 4). The structure has rigid connections in the nodes (the rods are welded in the nodes). Additionally, nuts are welded in the support nodes, which are used to attach the structure to the circumferential ring (one M12 bolt was used in each node to screw the structure, which simulates an articulated support). In order to reproduce the actual structure as accurately as possible in the numerical analyses, the model was carefully measured after being mounted on the test stand. Measurements were made of the length of the rods, the distance between the supports, and, treating the plane of the laser level as a reference level, the height of the individual nodes. In the tests, measurements were made of both the displacement of the central node (keystone) and the node of support no. 1. The displacements were measured using horizontal and vertical sensors. These sensors were placed at appropriate points of the structure to precisely monitor changes in displacements during loading. Five series of measurements allowed for accurate recording and analysis of deformations at different stages of the test. All structural elements of the stand are designed with precise measurement methods in mind, which ensure high accuracy of experimental results.

The tests used calibrated electronic sensors Mitutoyo Absolute ID-U with a measuring range of up to 25.4 mm and a resolution of 0.01 mm, measuring force < 1.8 N and a maximum permissible error of 0.02 mm. The load applied to the keystone was controlled for axiality before and during the test. It was applied manually using a hydraulic actuator, while it was read from a hook scale with a resolution of 1 N. The tests were

a)

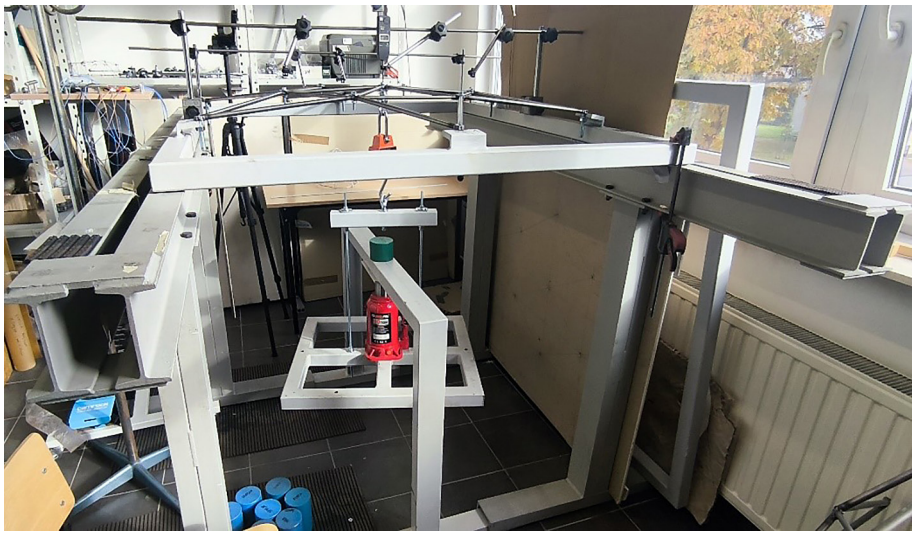

b)

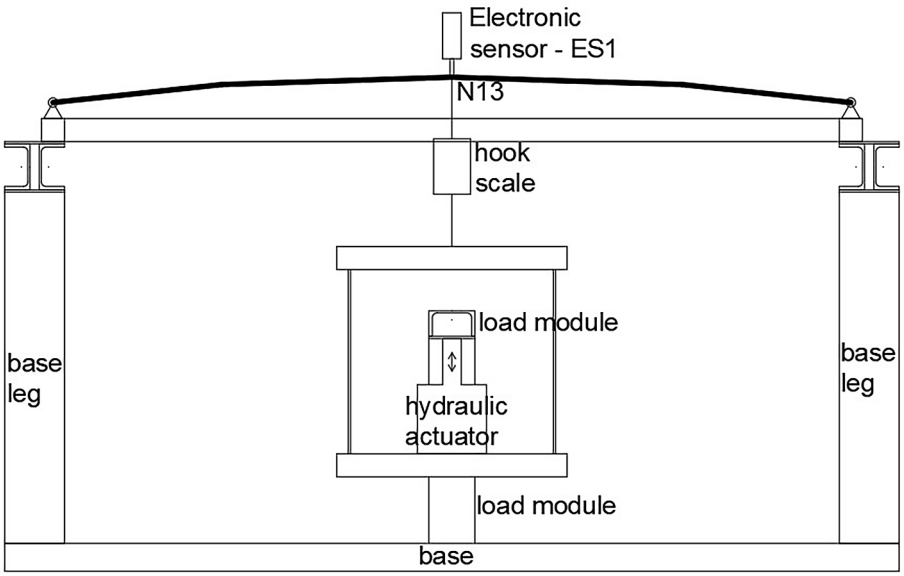

Figure 3. Experimental models test stand: (a) real view, (b) scheme

Table 1. Node coordinates

Low-rise dome					High-rise dome			
No. of Node	X [m]	Y [m]	Z [m]		No. of Node	X [m]	Y [m]	Z [m]
1	0.0000	-0.5280	- 0.0545		1	0.3090	-0.5270	- 0.1600
2	−0.5280	−0.3050	- 0.0560		2	-0.3090	-0.5270	- 0.1610
3	−0.5280	0.3050	- 0.0590		3	-0.6130	0.0057	- 0.1630
4	0.0000	0.5280	- 0.0565		4	-0.2980	0.5380	- 0.1630
5	0.5280	0.3050	- 0.0510		5	0.3070	0.5380	- 0.1580
6	0.5280	−0.3050	- 0.0505		6	0.6200	0.0030	- 0.1570
7	0.1480	−0.2560	- 0.0150		7	0.2600	-0.1420	- 0.0340
8	−0.1480	−0.2560	- 0.0155		8	0.0000	-0.2900	- 0.0390
9	−0.2960	0.0000	- 0.0190		9	-0.2530	-0.1470	- 0.0410
10	−0.1480	0.2560	- 0.0190		10	-0.2530	0.1530	- 0.0390
11	0.1480	0.2560	- 0.0150		11	0.0000	0.2900	- 0.0390
12	0.2960	0.0000	- 0.0160		12	0.2600	0.1530	- 0.0390
13	0.0000	0.0000	0.0000		13	0.0000	0.0000	0.0000

conducted under the same conditions: temperature 22 ° C +/- 1 ° C, humidity 50% +/- 5 %, which allowed to eliminate the influence of temperature changes on the accuracy of the measurements.

All of the above methods and measurements allow for precise verification of numerical analytical models and precise determination of the characteristics of deformations and the response of the structure to the applied load.

EXPERIMENTAL AND NUMERICAL RESULTS

Structure description

The article analyses the influence height to span ratio on the shape of the equilibrium path of the steel domes. Two types of steel domes consisting of 13 nodes and 24 bars were considered (Table 1). The structures differ in the height to span ratio: structure 1 – low-rise with H/S = 0.05 and structure 2 – high-rise with H/S = 0.13. The coordinates of the nodes were inventoried from the created models in order to compare the experimental results with the numerical results. The material parameters were verified in the experimental tests and included in the publication [37], i.e. E = 214.5 GPa, fy = 640 MPa. In the experimental model, individual steel bars were connected to each other by welded nodes. In order to reflect the experimental model, spatial frame elements were used in the numerical model. Figure 4 shows the appearance of experimental models for a low-rise dome (Figure 4a) and a high-rise dome (Figure 4b), respectively.

a)

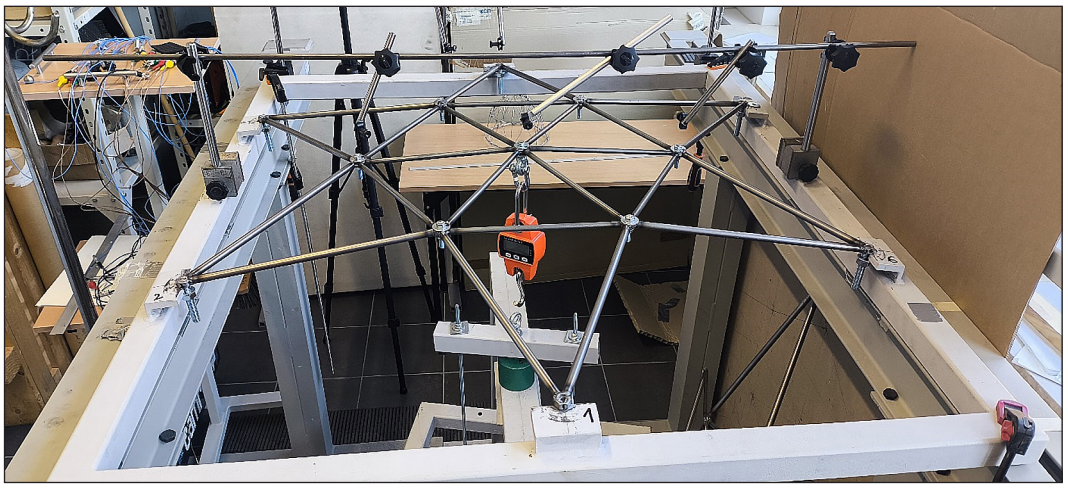

b)

Figure 4. Experimental model: (a) low-rise dome, (b) high-rise dome

First stage – experimental analysis

In the first stage, a series of experimental tests were performed. Figure 5 shows a comparison of the results for both types of structures: a low-rise dome and a high-rise dome. The graph shows significant differences in the nature and behavior of both structures. The equilibrium path for the high-rise dome is linear, while in the case of the low-rise dome, the shape of the equilibrium path clearly suggests non-linear behavior. The equilibrium paths for both structures were presented in the measurement range of the available devices (force up to about 3500 N and displacements up to about 20 mm). The maximum force values read for the high-rise dome are definitely higher than for the low-rise dome. They were: force 3419.83 N for a displacement of 2.03 mm in the case of the high dome and force 2680 N for a displacement of 15.96 mm in the case of the low-rise dome. At the same time, the displacement value for the high-rise dome was read in relation to a similar load value as in the case of the maximum load of the low-rise dome. This value was about 1.5 mm, which gives a more than 10-fold difference in the displacement values at the corresponding loads.

In order to estimate the accuracy of the measurements of the dome keystone displacements, the measurement uncertainty ranges were determined and the confidence intervals for the obtained results were determined. Type A uncertainty was determined based on repeated measurements of the same displacement value. The standard deviation of the sample was calculated and then the following formula was applied:

$$u_A = \frac{s}{\sqrt{n}} \tag{14}$$

where: s – standard deviation of the measurement series, n – number of repetitions performed.

The type B uncertainty was estimated based on the sensor manufacturer's data, possible calibration errors, nonlinearity of the measurement system and other systematic sources. The value of the maximum permissible error of the digital sensor was assumed: u_B =0.02 mm.

The total uncertainty was calculated as the square root of the sum of the squares of the type A and B uncertainties:

$$u_C = \sqrt{u_A^2 + u_B^2} \tag{15}$$

The expanded uncertainty and confidence interval were determined assuming a 95% confidence level (coverage factor k = 2): $U = k \bullet u_C$.

The confidence interval for the measured displacement at a 95% confidence level is: $x \pm U$, where x is the mean value of the measured displacement. The confidence interval results are presented in Tables 2 and 3.

Second stage – numerical analysis

Linear buckling analysis (LBA)

In the second stage, the results obtained from the experiment were compared with the results of the numerical analysis. The first step involved calculating the critical load multipliers using Linear Buckling Analysis. For the low-rise dome, the critical load factor was determined as $L_{cr,N}$=8.897 (Figure 6a), while for the high-rise dome, it was $L_{cr,W}$=17.374 (Figure 6b). According to design code guidelines, for low-rise structures ($L_{cr,N}$

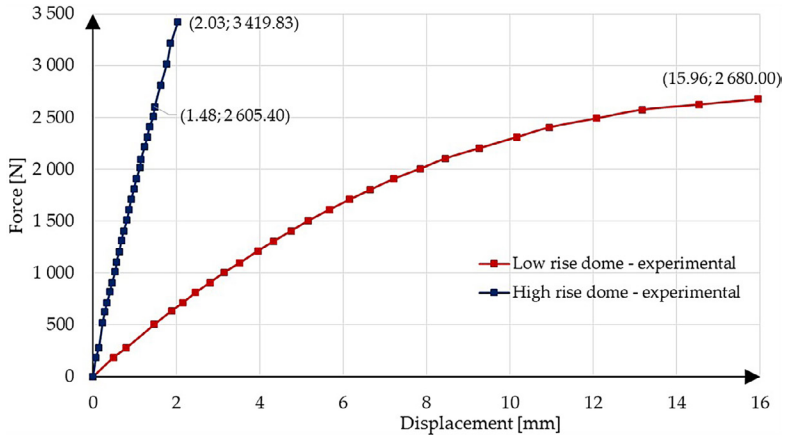

Figure 5. Equilibrium path for the experimental analysis case

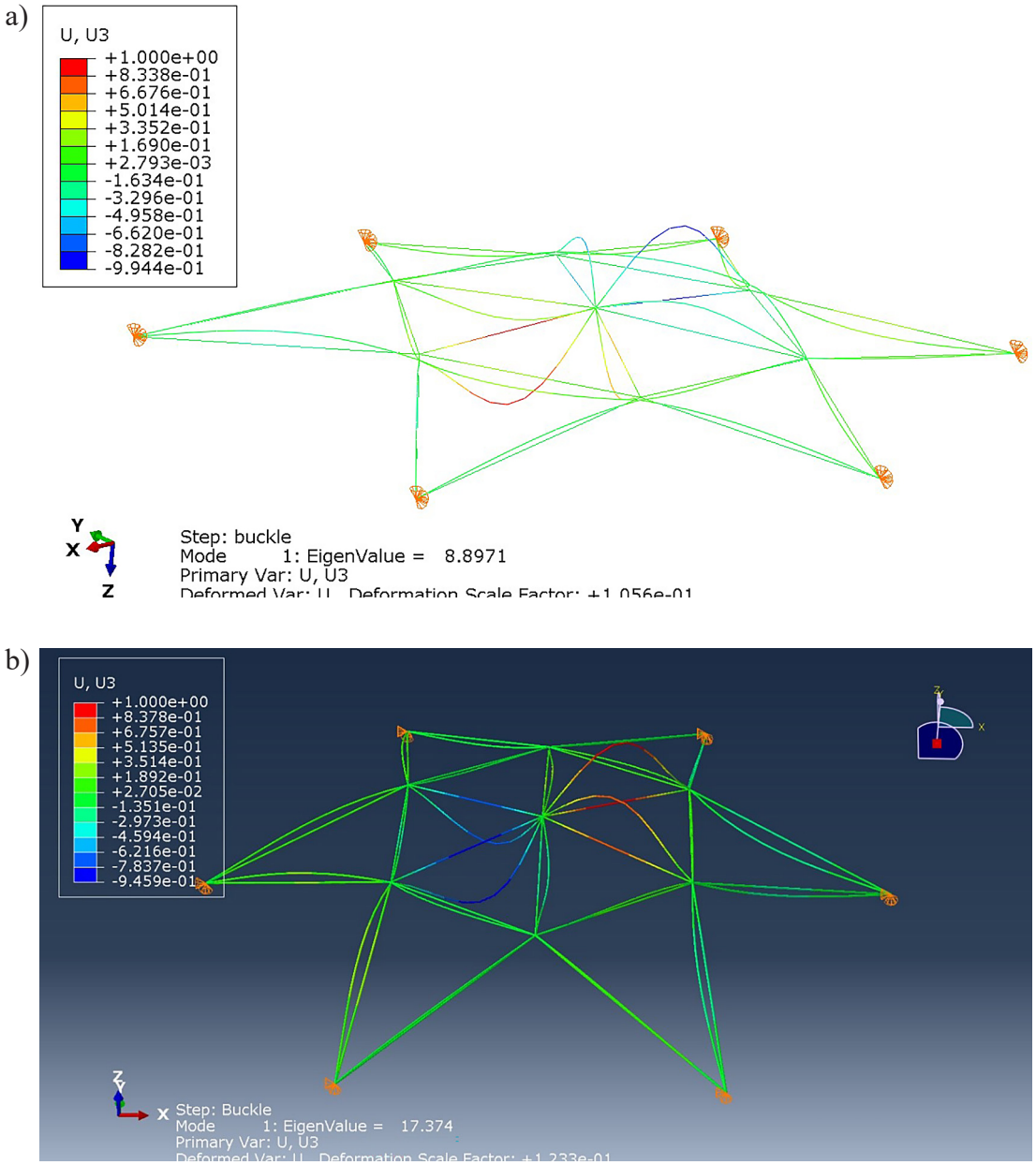

Figure 6. The first buckling mode of the LBA and the Eigenvalue: (a) low-rise dome, (b) high-rise dome

<10), it is recommended to use nonlinear analysis in further investigations.

Nonlinear analysis – standard approach

In the next step, based on measurements of the actual structure's geometry, node coordinates were entered into the SIMULIA Abaqus Learning Edition 2022 software. For both domes, nonlinear analyses were performed using the Riks arc-length method, which accounts for geometric nonlinearities and assumes linear elastic material behavior. Figure 7 presents graphs showing the relationship between the vertical displacement of the keystone and the applied load. Solid lines represent the experimental data, while dashed lines correspond to numerical results. Maximum values within the analysis range are indicated. The results reveal poor agreement between the numerical models and their experimental counterparts. Significant discrepancies were observed in both displacement values and the general shape of the load-displacement curves. During physical testing, slight displacements at the supports were noticed as the applied load increased. This observation led to a re-evaluation of support behavior and its influence on the structural equilibrium path. As a result, support flexibility was incorporated in the next phase of the numerical model.

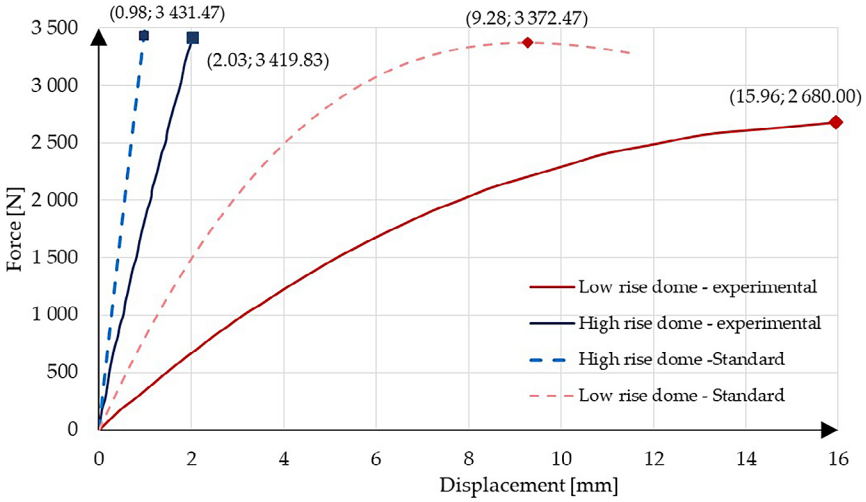

Figure 7. Comparison of equilibrium paths for the experimental and numerical analysis cases

Incorporating support flexibility

In the third step, support flexibility was introduced into the numerical model. Elastic foundation stiffness values were applied at each support: Kz = 1160 kN/m in the vertical (Z) direction and Kx = Ky = 35,000 kN/m in the horizontal (X and Y) directions. The results of this modification are shown in Figure 8. Although the new model captured some aspects of the observed behavior, the equilibrium path still differed considerably from the experimental results.

Incorporating support flexibility and geometric imperfections

In the final step of the analysis, both support flexibility and geometric imperfections were included. The *Imperfection command was used in the *Static Riks analysis module of Abaqus. This allowed the model to include a fraction of the first buckling mode shape, based on eigenvalue analysis. Since actual imperfections could not be measured, several imperfection amplitudes were considered, and the best-fitting values were selected:1% of the first mode for the low-rise dome and 0.5% for the high-rise dome. The results of these simulations are presented in Tables 2 and 3, and in Figure 9.

Based on the works [38, 39], it was observed that buckling of elements does not always lead to stability loss, and the phenomenon of node jump-through may be a decisive form of stability loss. During the present experimental tests, the loading time was short, and no time-dependent effects were observed. The values of von Mises stresses

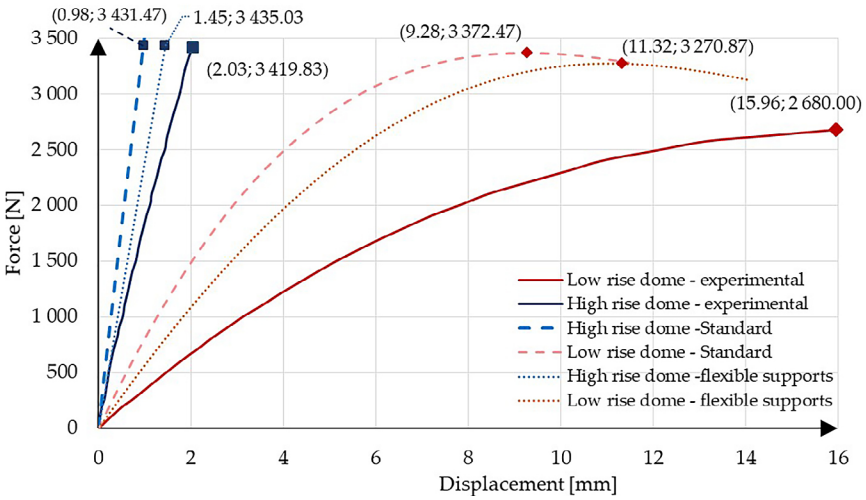

Figure 8. Comparison of equilibrium paths for the experimental, standard numerical, and flexible support cases

Table 2. Low-rise dome results

Low-rise dome experimental		Low-rise dome standard		Low-rise dome flexible supports (FS)		Low-rise dome FS + imperfection (IG) 1%	
Displacement [mm]	Force [N]	Displacement [mm]	Force [N]	Displacement [mm]	Force [N]	Displacement [mm]	Force [N]
0.00 ± 0.04	0.00	0.00	0.00	0.00	0.00	0.00	0.00
0.50 ± 0.04	187.27	0.22	186.95	0.32	186.45	0.49	186.13
0.80 ± 0.05	276.85	0.32	273.38	0.47	276.54	0.73	276.27
1.47 ± 0.12	503.17	0.60	506.30	0.88	503.09	1.38	504.17
1.89 ± 0.16	636.75	0.76	632.14	1.12	636.44	1.79	638.67
2.15 ± 0.10	712.80	0.87	711.30	1.27	713.07	2.03	714.38
2.46 ± 0.08	812.25	1.00	814.74	1.45	812.02	2.35	812.61
2.80 ± 0.07	907.17	1.13	907.44	1.64	907.03	2.67	907.74
3.15 ± 0.08	1008.50	1.27	1006.28	1.84	1008.02	3.02	1007.32
3.52 ± 0.07	1099.60	1.39	1094.78	2.02	1099.65	3.36	1099.68
3.95 ± 0.10	1213.60	1.57	1212.24	2.26	1214.39	3.80	1213.11
4.33 ± 0.09	1306.40	1.70	1303.56	2.45	1306.58	4.17	1304.69
4.75 ± 0.09	1407.80	1.86	1407.12	2.67	1406.59	4.62	1408.39
5.15 ± 0.08	1502.40	2.01	1500.45	2.88	1502.34	5.04	1500.94
5.68 ± 0.11	1613.67	2.20	1611.59	3.13	1613.28	5.57	1611.83
6.15 ± 0.08	1709.80	2.36	1705.49	3.36	1709.05	6.08	1710.54
6.65 ± 0.09	1804.00	2.53	1802.67	3.59	1804.28	6.59	1803.27
7.22 ± 0.14	1910.80	2.73	1908.56	3.85	1910.06	7.24	1911.12
7.85 ± 0.15	2007.00	2.92	2010.01	4.10	2007.00	7.88	2008.33
8.45 ± 0.20	2106.20	3.12	2107.07	4.37	2106.10	8.58	2105.63
9.26 ± 0.29	2204.83	3.32	2205.12	4.64	2204.72	9.37	2204.97
10.17 ± 0.41	2312.17	3.56	2313.51	4.96	2312.21	10.33	2311.66
10.95 ± 0.47	2406.80	3.78	2406.09	5.25	2406.19	11.30	2405.90
12.09 ± 0.49	2494.67	4.00	2493.59	5.54	2494.21	12.34	2494.31
13.17 ± 0.59	2577.25	4.22	2576.09	5.83	2577.52	13.44	2577.14
14.53 ± 0.55	2626.80	4.36	2625.68	6.01	2626.68	14.17	2626.77
15.96 ± 0.40	2680.00	4.52	2681.11	6.21	2680.56	15.02	2680.92

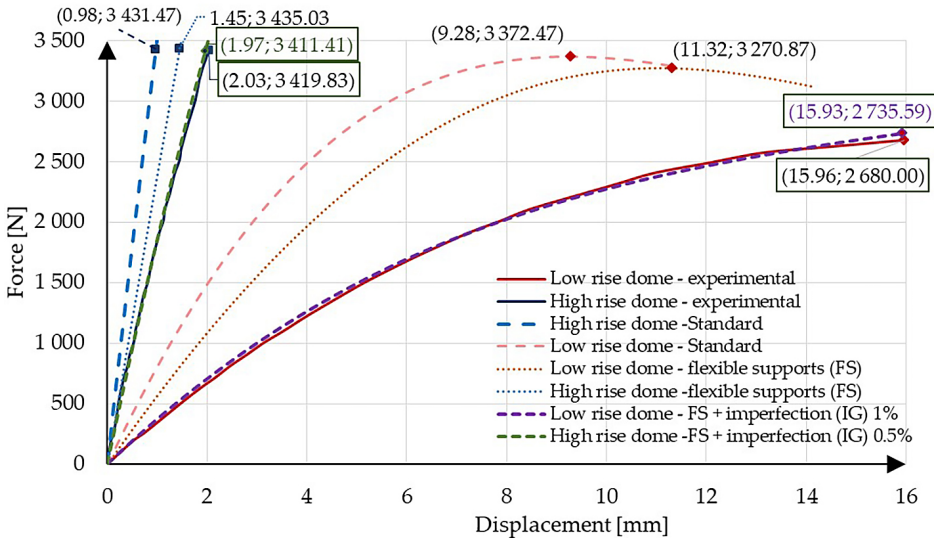

Figure 9. Comparison of equilibrium paths for the cases of experimental analysis, standard numerical analysis, and with flexible supports and with support flexibility and geometric imperfections

Table 3. High-rise dome results

High-rise dome experimental		High-rise dome standard		High-rise dome flexible supports (FS)		High-rise dome FS + imperfection (IG) 0.5%	
Displacement [mm]	Force [N]	Displacement [mm]	Force [N]	Displacement [mm]	Force [N]	Displacement [mm]	Force [N]
0.00 ± 0.04	0.00	0.00	0.00	0.00	0.00	0.00	0.00
0.14 ± 0.04	278.83	0.14	496.75	0.14	339.52	0.14	278.06
0.41 ± 0.04	818.33	0.41	1470.73	0.41	995.76	0.41	793.49
0.45 ± 0.04	907.80	0.46	1662.40	0.45	1094.86	0.45	860.46
0.53 ± 0.04	1009.83	0.54	1947.97	0.53	1292.78	0.53	1012.57
0.57 ± 0.04	1108.60	0.57	2042.63	0.57	1381.73	0.57	1088.10
0.63 ± 0.04	1205.80	0.62	2231.19	0.63	1529.81	0.63	1191.39
0.68 ± 0.04	1313.40	0.68	2418.70	0.68	1648.13	0.68	1284.71
0.73 ± 0.04	1406.50	0.73	2605.18	0.73	1766.31	0.73	1377.47
0.82 ± 0.04	1511.00	0.81	2882.95	0.82	1982.62	0.82	1533.88
0.86 ± 0.04	1608.80	0.87	3066.83	0.86	2070.97	0.86	1606.92
0.92 ± 0.04	1712.50	0.92	3249.67	0.92	2218.06	0.92	1706.75
0.98 ± 0.04	1809.00	0.98	3431.47	0.98	2355.15	0.98	1814.87
1.04 ± 0.04	1915.00	1.03	3612.24	1.04	2492.04	1.04	1922.15
1.13 ± 0.04	2020.67	1.14	3970.66	1.13	2706.76	1.13	2072.68
1.15 ± 0.04	2100.50	1.16	4059.61	1.15	2755.49	1.15	2107.86
1.24 ± 0.04	2218.40	1.25	4324.93	1.24	2969.61	1.24	2264.95
1.30 ± 0.04	2313.60	1.30	4500.51	1.30	3105.61	1.30	2360.00
1.36 ± 0.04	2412.80	1.35	4675.06	1.36	3231.71	1.36	2462.86
1.45 ± 0.04	2512.17	1.46	5021.06	1.45	3444.70	1.45	2607.08
1.48 ± 0.04	2605.40	1.49	5106.91	1.48	3512.36	1.48	2657.56
1.62 ± 0.04	2813.00	1.62	5532.29	1.62	3840.25	1.62	2881.98
1.77 ± 0.05	3015.67	1.78	6034.24	1.77	4176.44	1.77	3117.98
1.87 ± 0.04	3215.80	1.86	6281.74	1.87	4406.17	1.87	3269.74
2.03 ± 0.06	3419.83	2.03	6769.79	2.03	4768.55	2.03	3512.45

for the low-rise dome in the most stressed bars for the last points on the equilibrium path (Figure 9) with coordinates (15.93; 2735.59) were 139.5 MPa. In the case of the high-rise dome for the point (1.97, 3411.41) (Figure 8) they were 86.35 MPa. The yield stress is fy = 235 MPa. The use of linear physical relations (taking into account the elastic work of the structure) was justified. Sensitivity analysis is extremely useful for assessing the impact of variability of individual input parameters on the final outcome of the model or decision [40, 41]. Additionally, a simplified sensitivity analysis

Table 4. Low-rise dome sensitivity results

Reference values Flexible support Imperfection 1%		Taking into account the change of imperfections Δ_δ = 0.1%		Sensitivity to change in % imperfection	Taking into account the change in support flexibility Δ_{Ks} = 10%		Sensitivity to change in % flexibility
Displacement [mm]	Force [N]	Displacement [mm]	Force [N]	$\frac{U_{\delta+} - U_0}{\Delta_\delta}$	Displacement [mm]	Force [N]	$\frac{U_{K+} - U_0}{\Delta_{Ks}}$
3.01	1003.56	3.18	1003.08	166.21	2.96	1004.84	-0.047
5.02	1497.92	5.32	1498.2	294.57	4.94	1501.82	-0.067
7.80	1997.68	8.28	1998.38	472.72	7.67	1998.62	-0.119
12.42	2500.31	13.01	2499.3	598.7	12.19	2500.87	-0.197
15.93	2735.59	16.32	2734.76	390.6	15.63	2735.85	-0.262

Table 5. High-rise dome sensitivity results

Reference values Flexible support Imperfection 0.5%		Taking into account the change of imperfections Δ_δ = 0.1%		Sensitivity to change in % imperfection	Taking into account the change in support flexibility Δ_{Ks} = 10%		Sensitivity to change in % flexibility
Displacement [mm]	Force [N]	Displacement [mm]	Force [N]	$\frac{U_{\delta+} - U_0}{\Delta_\delta}$	Displacement [mm]	Force [N]	$\frac{U_{K+} - U_0}{\Delta_{Ks}}$
0.53	1003.1	0.58	1006.97	50.241	0.51	1001.51	-0.0079
1.09	2002.05	1.19	1997.03	104.31	1.07	2004.48	-0.0140
1.39	2505.46	1.53	2503.27	141.92	1.36	2503.94	-0.0191
1.69	2996.56	1.88	3000.84	186.15	1.66	2998.49	-0.0216
1.97	3419.22	2.19	3420.42	222.45	1.93	3416.29	-0.0266

Table 6. Relative errors in case low-rise dome

Load [N]	Relative Error		
	Experimental—Standard analysis [%]	Experimental—Numerical analysis with flexible supports [%]	Experimental—Numerical analysis with flexible supports taking into account 1% of imperfection [%]
0.00	0.0	0.0	0.0
187.27	56.4	36.0	1.9
276.85	59.9	40.3	7.9
503.17	58.9	40.2	5.8
636.75	59.6	40.6	5.1
712.80	59.7	41.1	5.5
812.25	59.2	40.9	4.4
907.17	59.6	41.5	4.5
1008.50	59.8	41.7	4.0
1099.60	60.4	42.6	4.5
1213.60	60.4	42.9	3.8
1306.40	60.7	43.4	3.6
1407.80	60.8	43.8	2.8
1502.40	60.9	44.1	2.3
1613.67	61.3	44.9	1.9
1709.80	61.7	45.4	1.2
1804.00	61.9	46.1	0.8
1910.80	62.3	46.7	0.3
2007.00	62.8	47.7	0.4
2106.20	63.1	48.3	1.5
2204.83	64.1	49.9	1.2
2312.17	64.9	51.2	1.6
2406.80	65.5	52.1	3.2
2494.67	66.9	54.2	2.1
2577.25	68.0	55.7	2.1
2626.80	70.0	58.7	2.5
2680.00	71.7	61.1	5.9

was performed. The vertical displacement of the keystone joint U_Z was defined as a function of two variables $U_Z = f(\delta, K_s)$. The first variable was the amplitude of the geometric imperfection δ. The second variable was the elasticity of the supports K_s. The reference point was the calculations for the situation in which the support flexibility and the imperfection values of 0.5% for the high

Table 7. Relative errors in case high-rise dome

Load [N]	Relative Error		
	Experimental —Standard analysis [%]	Experimental— Numerical analysis with flexible supports [%]	Experimental— Numerical analysis with flexible supports taking into account 0.5% of imperfection [%]
0.00	0.0	0.0	0.0
278.83	41.1	17.3	3.4
818.33	47.0	18.1	4.8
907.80	45.7	17.1	5.8
1009.83	43.8	22.1	0.2
1108.60	42.4	19.6	3.2
1205.80	43.6	20.7	2.3
1313.40	44.3	20.6	2.2
1406.50	44.4	21.0	2.2
1511.00	46.8	23.5	0.8
1608.80	46.3	22.6	0.2
1712.50	46.6	22.3	0.9
1809.00	47.3	23.5	0.3
1915.00	47.9	23.8	0.5
2020.67	49.5	25.6	2.6
2100.50	48.1	24.1	0.4
2218.40	49.6	25.4	1.6
2313.60	49.8	25.7	1.8
2412.80	50.0	25.8	1.8
2512.17	51.2	27.6	3.6
2605.40	50.5	26.4	2.0
2813.00	51.4	27.2	2.3
3015.67	50.9	28.5	3.6
3215.80	50.7	27.8	1.8
3419.83	52.0	29.3	3.1

structure and 1% for the low structure were assumed: $U_0 = f(\delta_0, K_{s0})$. Then, small parameter increments equal to $\Delta_\delta = 0.1\%$ for the imperfection and $\Delta_{Ks} = 10\%$ for the flexibility were determined. Numerical analyses were performed in Abaqus for the following cases: $U_{\delta+} = f(\delta_0+\Delta_\delta, K_{S0})$ and $U_{K+} = f(\delta_0, K_{S0}+\Delta_{Ks})$. In the last step, partial derivatives were calculated in an approximate way for five different points of the equilibrium path. Partial derivatives were determined using the approximation: $\frac{\partial U_Z}{\partial \delta} \approx \frac{U_{\delta+}-U_0}{\Delta\delta}$, $\frac{\partial U_Z}{\partial K_s} \approx \frac{U_{K+}-U_0}{\Delta K_s}$. The sensitivity analysis helped to prioritize the modelling efforts for practical applications. Geometric imperfections have a much greater impact on improving the results. The results are presented in Tables 4 and 5. In order to better illustrate the differences between subsequent stages for both the low-rise and the high-rise dome, relative errors are presented in Table 6 and 7.

DISCUSSION

Two types of domes were analyzed: a low-rise dome and a high-rise dome. The experimental responses were compared with numerical simulation results for three variants: standard model (rigid supports, no imperfections), model with flexible supports (FS), model with flexible supports and a geometric imperfection (FS + IG). The difference in the node displacement for the standard approach between the ideal and experimental model of the structure was: for a load of 2680 N about 11.4 mm in the case of a low-rise structure and for a load of about 2600 N about 0.75 mm in the case of a high-rise structure. Consideration of the estimated support flexibility influenced the numerical results, reducing the maximum displacement discrepancy in the keystone to approximately 10 mm for a

low-rise structure and about 0.39 mm for a high-rise structure. The differences between the experimental and numerical results taking into account the support flexibility are still noticeable (relative errors for such a solution range from about 26% to about 61%). The next step was to consider the % eigenvalues of the first eigenvalue from the buckling analysis. This approach demonstrated that the numerical results closely matched the experimental data. The maximum displacement error between the experimental and numerical results, considering imperfections, was approximately 11.8% (load of about 276 N) for the low-rise structure and about 15% for the high structure (load of about 500 N). The inclusion of flexible supports and imperfections in numerical models of bar domes was crucial to accurately represent the actual behavior of the structure under load.

CONCLUSIONS

This article presents the results of experimental tests and numerical analyses of two steel domes differing in height. The study aimed to calibrate a numerical model by including geometric nonlinearities and fabrication imperfections to match experimental results. The simulations were performed in the Abaqus environment using the Riks method, enabling the capture of buckling and snap-through behavior and the full equilibrium path in the instability region.

Initially, numerical results significantly differed from experimental measurements. After identifying the causes of these discrepancies, two key factors were addressed: the elastic behavior of supports and geometric imperfections. Including these aspects resulted in a high degree of agreement between the simulation and test results.

For the high-rise dome the equilibrium path is linear over the entire load range, whereas for the low-rise dome the course is clearly non-linear. Detailed engineering recommendations:

- support modeling: numerical models should use elastic supports that reflect the real compliance of the structure.
- inclusion of imperfections: geometric imperfections should be introduced using the first buckling mode with an appropriate amplitude (e.g., 0.5–1%).
- model validation: numerical models must be validated through physical testing, especially when dealing with instability phenomena.
- use of Riks method: for nonlinear analysis of dome structures, the Riks method should be preferred over standard static analyses.
- sensitivity analysis: even minor geometric imperfections significantly affect the global response of structures, especially those susceptible to buckling.

REFERENCES

1. Lan TT. Space frame structures. In: Chen W-F, Lui EM, editors. Handbook of Structural Engineering. 2nd ed. Boca Raton (FL): CRC Press; 2005.
2. Makowski ZS. Analysis, Design and Construction of Braced Barrel Vaults. London (UK): Taylor & Francis; 2006.
3. Chilton J. Space Grid Structures. Oxford (UK): Architectural Press; 2000.
4. Szmit R. Design and analysis of steel single-layer cylindrical roofs. Przegląd Budowlany. 2021;92:73–6.
5. Steel structures with large spans [Internet]. [Available online 2025 Mar 31]. https://www.izbudujemy.pl/artykuly/452/Konstrukcje-stalowe-o-duzych-rozpietosciach
6. Kowolik B. Steel structures of large-scale halls. Nowoczesne Hale. 2019;2:48–53.
7. Shen J, Groh RMJ, Schenk M, Pirrera A. Experimental path-following of equilibria using Newton's method. Part I: Theory, modelling, experiments. Int J Solids Struct. 2021;210–211:203–23.
8. Guan Y, Virgin LN, Helm D. Structural behavior of shallow geodesic lattice domes. Int J Solids Struct. 2018;155:225–39.
9. Silveira RAM, Nogueira ChL, Gonçalves PB. A numerical approach for equilibrium and stability analysis of slender arches and rings under contact constraints. Int J Solids Struct. 2013;50:147–59.
10. Li W, Zhi X, Wang D, Fan F, Shen S. Static stability analysis of a reticulated shell with a roofing system. Eng Struct. 2019;185:315–31.
11. Li P, Wu M, Xing P. Novel cable-stiffened single-layer latticed shells and their stabilities. J Constr Steel Res. 2014;92:114–21.
12. Li YG, Fan F, Hong HP. Reliability of lattice dome with and without the effect of using small number of ground motion records in seismic design. Eng Struct. 2017;151:381–90.
13. Ma H, Ma Y, Yu Z, Fan F. Experimental and numerical research on gear-bolt joint for free-form grid spatial structures. Eng Struct. 2017;148:522–40.

14. Zhu Z-C, Luo Y-F, Xiang Y. Global stability analysis of spatial structures based on Eigen-stiffness and structural Eigen-curve. J Constr Steel Res. 2018;141:226–40.
15. Xu Y, Han Q-H, Parke GAR, Liu Y-M. Experimental study and numerical simulation of the progressive collapse resistance of single-layer latticed domes. J Struct Eng. 2017;143(9):04017121.
16. Silva WTM, Ribeiro KQ. Spatial asymmetric/symmetric buckling of Mises truss with out-of-plane lateral linear spring. Int J Non-Linear Mech. 2021;137:103810.
17. Yan S, Zhao X, Rasmussen KJR, Zhang H. Identification of critical members for progressive collapse analysis of single-layer latticed domes. Eng Struct. 2019;188:111–20.
18. Kala Z. Computation of equilibrium paths in nonlinear finite element models. MATEC Web Conf. 2016;7:04026.
19. Hrinda GA. Snap-through instability patterns in truss structures. In: 51st AIAA/ASME/ASCE/AHS/ASC Structures, Structural Dynamics, and Materials Conference, 18th AIAA/ASME/AHS Adaptive Structures Conference, 12th. Orlando (FL), USA; 2010 Apr 12–15.
20. Radoń U, Zabojszcza P, Sokol M. The influence of dome geometry on the results of modal and buckling analysis. Appl Sci. 2023;13:2729. https://doi.org/10.3390/app13042729
21. Hammar I, Djermane M, Amieur B. Dynamic buckling analysis of ductile damage evolution for thin shell with Lemaitre's model. Civ Eng J. 2024;10(3).
22. Shen L, Gao Y, He M, Du N. Finite element parameter analysis of bearing capacity and plastic deformation in two-segment replaceable link with a separated splicing plate of LYP160 steel. Structures. 2025;73:108408. https://doi.org/10.1016/j.istruc.2025.108408
23. Riks E. An incremental approach to the solution of snapping and buckling problems. Int J Solids Struct. 1979;15:529–51.
24. Riks E. The application of Newton's method to the problem of elastic stability. J Appl Mech. 1972;39:1060–5.
25. Wempner GA. Discrete approximation related to nonlinear theories of solids. Int J Solids Struct. 1971;7:1581–99.
26. Batoz JL, Dhatt G. Incremental displacement algorithm for nonlinear problems. Int J Numer Methods Eng. 1979;14:1262–7.
27. Crisfield MA. A fast incremental/iterative solution procedure that handles snap-through. Comput Struct. 1981;13:55–62.
28. Crisfield MA. Variable step-lengths for nonlinear structural analysis. TRR Lab Rep. 1982;1049.
29. Crisfield MA. Snap-through and snap-back response in concrete structures and the dangers of under integration. Int J Numer Methods Eng. 1986;22:751–67.
30. Ramm E. Strategies for tracing the non-linear response near limit points. In: Nonlinear Finite Element Analysis in Structural Mechanics. Berlin/Heidelberg (Germany): Springer; 1981. p. 63–89.
31. Powell G, Simons J. Improved iterative strategy for nonlinear structures. Int J Numer Methods Eng. 1981;17:1455–67.
32. Bathe KJ, Dvorkin EN. On the automatic solution of nonlinear finite element equations. Comput Struct. 1983;17:871–9.
33. Park KC. A family of solution algorithms for nonlinear structural analysis. Int J Numer Methods Eng. 1982;18:1337–47.
34. Giżejowski M, Szczerba R, Gajewski M. FEM models and simulation methods in the analysis of lateral-torsional buckling of steel structural elements. J Civ Eng Environ Archit. 2016;33(63):339–46.
35. Zabojszcza P, Radoń U. Effect of increased density of nodes in geodesic dome on its critical load capacity. In: 3rd WMCAUS 2018;471.
36. Radoń U. Numerical aspects of application of FORM in node snapping truss structures. Arch Civ Mech Eng. 2015;15(1):262–71.
37. Zabojszcza P, Radoń-Kobus K, Kossakowski PG. Verification of numerical models of steel bar coverings using experimental tests—preliminary study. Metals. 2024;14:1319. https://doi.org/10.3390/met14121319
38. Opatowicz D, Radoń U, Zabojszcza P. Assessment of the effect of wind load on the load capacity of a single-layer bar dome. Buildings. 2020;10:179.
39. Zabojszcza P, Radoń U. Optimization of steel roof framing taking into account the random nature of design parameters. Materials. 2022;15(14):5017 https://doi.org/10.3390/ma15145017
40. Radoń U, Zabojszcza P. The application of structural reliability and sensitivity analysis in engineering practice. Appl Sci. 2025;15:342. https://doi.org/10.3390/app15010342
41. Zhou Y, Tian H, Hu D, Hu H, Shen Q. Spatial-temporal characteristics of green development level in river basin. HighTech Innov J. 2024;5(4):1068–84. https://doi.org/10.28991/HIJ-2024-05-04-014